# Anomaly detection of man-made objects using spectro-polarimetric imagery

Brent D. Bartlett and Ariel Schlamm and Carl Salvaggio and David W. Messinger

Rochester Institute of Technology, Chester F. Carlson Center for Imaging Science, Digital Imaging and Remote Sensing Laboratory, Rochester, NY, USA

## ABSTRACT

In the task of automated anomaly detection, it is desirable to find regions within imagery that contain man-made structures or objects. The task of separating these signatures from the scene background and other naturally occurring anomalies can be challenging. This task is even more difficult when the spectral signatures of the man-made objects are designed to closely match the surrounding background. As new sensors emerge that can image both spectrally and polarimetrically, it is possible to utilize the polarimetric signature to discriminate between many types of man-made and natural anomalies. One type of passive imaging system that allows for spetro-polarimetric data to be collected is the pairing of a liquid crystal tunable filter (LCTF) with a CCD camera thus creating a spectro-polarimetic imager (SPI). In this paper, an anomaly detection scheme is implemented which makes use of the spectral Stokes imagery collected by this sensing system. The ability for the anomaly detector to find man-made objects is assessed as a function of the number of spectral bands available and it is shown that low false alarm rates can be achieved with relatively few spectral bands.

**Keywords:** spectro-polarimetric, anomaly detection, hyperspectral, multispectral, polarization

## 1. INTRODUCTION

As remote sensing continues to evolve, hardware advances have allowed for sensing systems to collect vast amounts of data. While this data promises to hold a wealth of information about the world, new approaches are needed to automatically analyze and present information that is relevant to the solution for particular problems. One approach to dealing with large data sets is to process the data looking for anomalies which can then be used to cue an analysts, thus saving costly manual search time.[1] In the context of this study, an anomaly is defined as an object that is man-made while being surrounded by a natural background. A sensing modality that holds potential for solving this type of task is to capture not only the spectral content, but the wave nature of light as well by using sensing systems that record the polarization state of reflected radiation. While several approaches using active sources of polarized illumination show promise,[2,3] this work will focus on processing passive polarimetric imaging. It has been noted that passive imagery, spectral information is dependent on the materials molecular make-up while the polarization state of the sensed radiance is due primarily to the object geometry and surface properties.[4] This means that there is the potential to increase the information contained in imagery that has both spectral and polarimetric content.

It has been shown that data from spectral sensors can be fused with polarimetric data to achieve lower false alarm rates than using a single modality, depending on different parameters such as scene and collection geometries, background clutter, and fusion approaches.[5] This paper will apply spectral algorithms to data that is both spectral and polarimetric due to the method in which it was collected, termed spectro-polarimetric. A system capable of collecting this data that is based on a liquid crystal tunable filter (LCTF) has been used to collect spectro-polarimetric data and retrieve p-brdf of in-scene materials.[6] This system produces data that is similar to typical hyperspectral data but instead of a single cube of image data there are three image cubes each corresponding to a different element of the Stokes vector.

One way to process data to produce a single stacked image cube for which standard spectral algorithms can be applied will be shown. Applying an anomaly detection routine to this stacked polarimetric image cube has been shown to reduce the number of false alarms for the task of finding anomalous man-made objects over several different ground sample distances.[7] This paper will explore how spectrally resampling spectro-polariemtric data of a scale model test scene collected in the laboratory will impact the performance of an anomaly detection routine to suppress false alarms due to natural background objects. This type of analysis can help guide the development of new spectro-polarimetric imager designs that require multispectral resolution due to system constraints.

Further author information: E-mail: bartlett@cis.rit.edu, Telephone: 1 585 475 5037

Algorithms and Technologies for Multispectral, Hyperspectral, and Ultraspectral Imagery XVII, edited by Sylvia S. Shen, Paul E. Lewis, Proc. of SPIE Vol. 8048, 80480B · © 2011 SPIE
CCC code: 0277-786X/11/$18 · doi: 10.1117/12.884167

## 2. APPROACH AND THEORY

This work analyzes the application of a spectral anomaly detection routine on spectro-polarimetric data collected in the laboratory of a scale model scene. The test data that is collected is calibrated to sensor reaching radiance through the use of a calibrated light source, which will correct the imagery for non-uniformities across the image plane. The imagery collected at each polarimetric filter position is registered to account for spatial shifting caused by the rotation of the LCTF in front of the camera. The image data at each filter orientation is then combined to produce Stokes imagery using a modified Pickering Method[4] as given by

$$\begin{aligned} S_0 &= \frac{(L_0 + L_{45} + L_{90} + L_{135})}{2} \\ S_1 &= L_0 - L_{90} \\ S_2 &= L_{45} - L_{135} \end{aligned} \tag{1}$$

where $S_0$, $S_1$, and $S_2$ are Stokes imagery, and $L_0$,$L_{45}$,$L_{90}$,$L_{135}$ are radiance images at each of the four filter orientations where each Stokes image is a function of wavelength.

At this point traditional spectral tools can be applied either directly or to combinations of the Stokes image cubes. To take advantage of the polarimetric data, one large data set can be formed by stacking each Stokes cube to create a single cube with three times the number of spectral bands. Before doing this, the S0 band must be scaled to lie in the same relative data range as the S1 and S2 images so that the spectral algorithms are not dominated by the S0 information. This can be accomplished for most scenes by simply de-meaning the S0 cube since S1 and S2 data of typical remote sensing scenes have a mean close to zero. This type of data combination will be referred to as simply S0S1S2. The entire process is outlined in Figure 1.

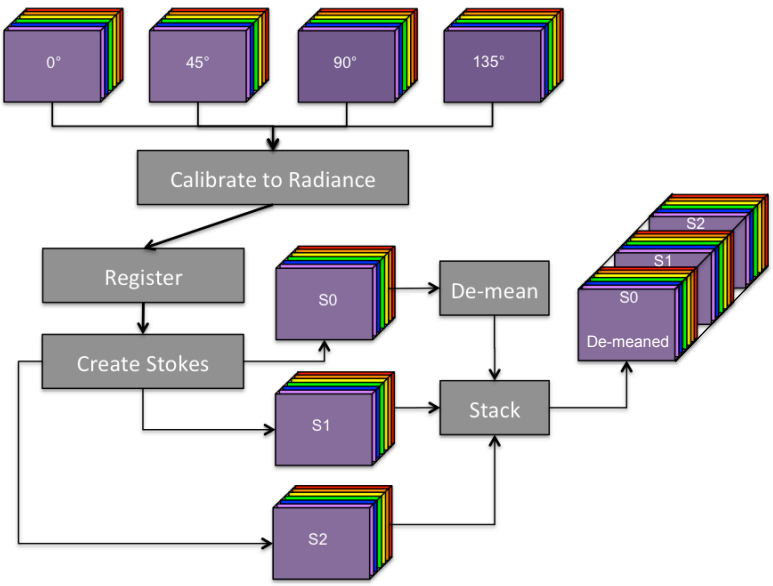


Figure 1: Processing steps used to create final spectro-polarimetric data product.

### 2.1 Scene Data

The system used to collect data for this study generates spectro-polarimetric data by rotating a LCTF in front of a gigabit ethernet camera. Since this system collects spectro-polarimetic data, it is termed a spectro-polarimetic imager (SPI). The LCTF can electronically scan a 7nm spectra bandpass from 450 to 720nm. The LCTF also acts as a linear polarizer which provides polarimetric filtering which has been used to form spectro-polarimetric image cubes.[6,7] This system was used to collect data of a scale model scene in the laboratory. The scene was imaged four times to collect data of a Humvee, a tank, a green car, and the background. These images were then tiled and down-sampled back to the original image size. This

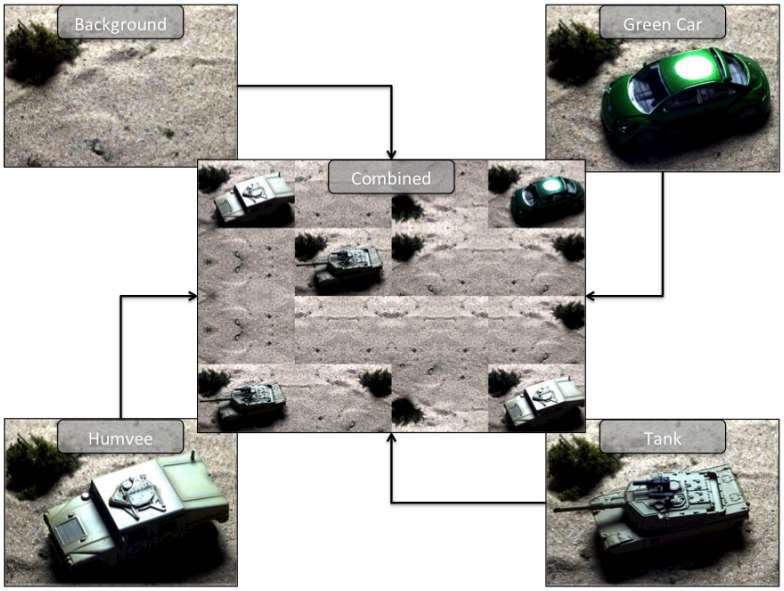

Figure 2: Imagery created by collecting data of a scale model desert scene. Imagery was combined and resampled to create composite image that contains multiple targets and background.

produced a single scene containing a mixture of background and target objects at a larger relative ground sample distance (GSD) than the original capture resolution. The original and combined imagery are shown in Figure 2.

Because the purpose of this study is to explore the effects of only spectral sampling, the scene geometry was chosen to maximize the polarimetric contrast and provide a best case detection scenario. However, it should be noted that these these results do in general depend on source / target / sensor geometry. Different geometric configurations may produce different results with this type of data. The scene with large area source, scale model scene, and sensor is shown in Figure 3 and shows the placement of the sensor in the principle plane of the source with a zenith angle of $45°$.

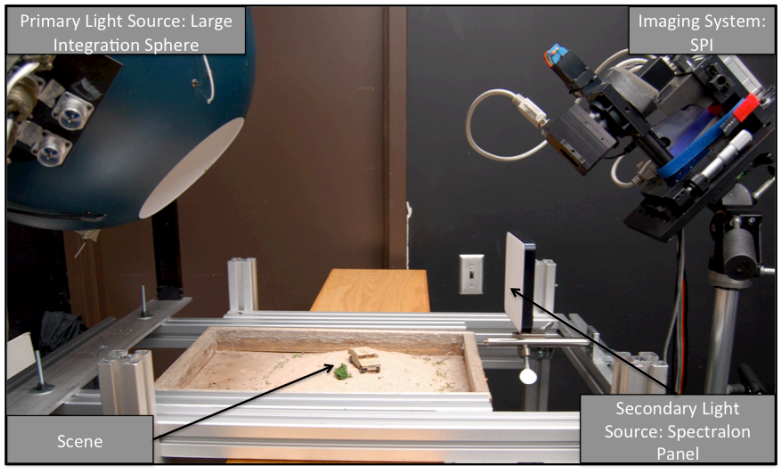

Figure 3: Image of laboratory setup showing the integrating sphere used as primary light source, the Spectralon panel which provides a secondary light source through reflection, and the SPI.

Each image cube was then resampled spectrally to determine what effect the number of bands has on the algorithm performance. The LCTF imagery has a spectral spacing of 10nm over the spectral range of 450-720nm. The system response was then resampled to have 14 bands with a full width half max of 14nm, the 4 visible bands of the WorldView 2 (WV2) satellite, 3 RGB bands matching a Sony color CCD response, and the single panchromatic WV2 band. These bands are all based on actual system response functions and are shown in Figure 4.

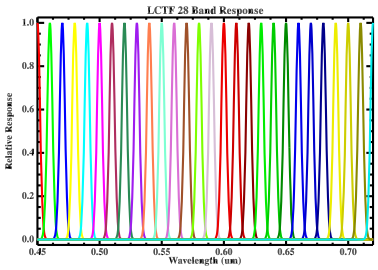


(a) Original LCTF spectral response.

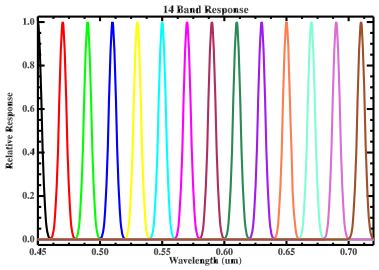


(b) 14 band spectral response.

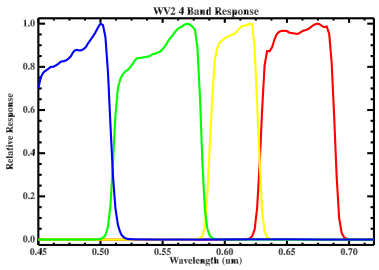


(c) Four of the WorldView 2 spectral bands.

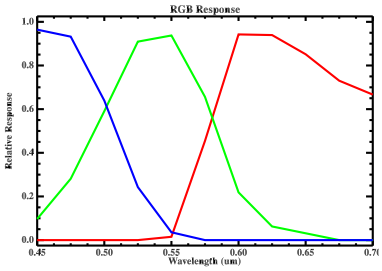


(d) RGB bands of a typical Sony CCD color array.

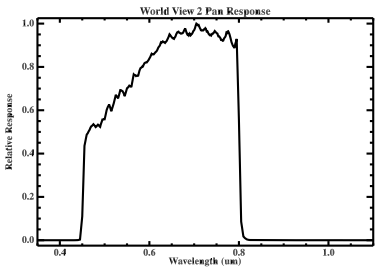


(e) Panchromatic band from the WorldView 2 satellite.

Figure 4: Different spectral responses chosen for resampling of image cubes.

## 2.2 Anomaly Detection

Once the scale model scene imagery has been acquired and processed, anomaly detection can be performed. The most commonly used anomaly detection routine is the the RX algorithm,[8]

$$R(\mathbf{x}) = (\mathbf{x} - \mathbf{m})^T \mathbf{\Sigma}^{-1} (\mathbf{x} - \mathbf{m}), \tag{2}$$

where $\mathbf{x}$ is the pixel spectral vector, $\mathbf{m}$ is the mean spectral vector, and $\mathbf{\Sigma}$ is the covariance of the distribution. Essentially, the RX algorithm computes the Mahalanobis distance from each pixel to the spectral distribution of the global image. When this distance is small, the pixel is within the background variability of the data. A large $R(\mathbf{x})$ score corresponds to points that are more distant from the background and therefore more anomalous. The $R(\mathbf{x})$ value is typically thresholded to create a binary detection map. This is a statistical detector with a constant false alarm rate (CFAR), which is based on the assumption that the background is normally distributed and that the anomalies have some additive spectral feature relative to the background.[9]

The Topological Anomaly Detector (TAD), is a data driven approach to anomaly detection that describes the background distribution of the data in terms of a simplicial complex or a graph. Points are connected to their nearest neighbors, in terms of Euclidean distance, to build the background components. Points that are not connected to a background component in the simplicial complex are anomalous which can been seen in Figure 5(a). Typically, the average Euclidean distance to the nearest few points on a background component, or the co-density distance, is calculated and used as the anomalous score. This metric produces different results in comparison to calculating a points Euclidean distance relative to a background mean, which is shown in Figure 5(b).

For this application, a hybrid approach between RX and TAD (TAD-RX) is used for anomaly detection. The covariance matrix in RX is computed using only those points that are assigned into the background using TAD. Then the standard RX score is computed per pixel. Using the TAD anomaly removed background covariance matrix has been shown to provide improved results in statistical target detection approaches[11,12] by removing the anomalous pixels from influencing the background covariance matrix.

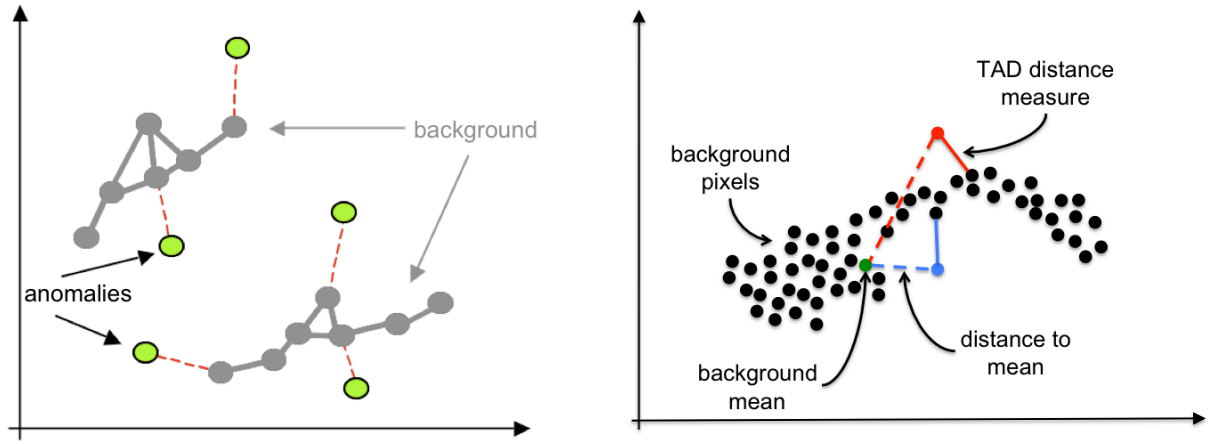


(a) Anomalies as defined by TAD.

(b) TAD distance differs from distance to mean.

Figure 5: Visualization of two notional point clouds showing how TAD calculates distance and defines anomalies.

For this experiment, the hardest object to distinguish from the background is the tank. This is due to its spectral signature being very similar to that of the sand background as well as it's complex surface geometry which tends to decrease the polarimetric signal. Comparatively, the large flat panels of the Humvee and the glossy finish of the car produce good polarimetric contrast to that of the background. The TAD-RX result is therefore thresholded so at least $25\%$ of the tank pixels are classified as anomalous, which will allow for a fair comparison between spectrally resampled images. This was accomplished by creating several regions of interests (ROI) that contain the pixels of each of the scale model vehicles. The number of true detections is then found by counting the number of anomalous pixels detected that fall within the area known to contain the target. The number of false alarms is found by counting the number of pixels that do not contain the known targets. The false alarm rate is used as the comparison metric for this analysis.

## 3. RESULTS

TAD-RX, the anomaly detection routine used here, produces a map where the value for each pixel is the RX measure of anomalousness relative to the TAD-anomaly removed background. The thresholded result can then be viewed as an image which gives a visual sense of the results. These images are shown in Figure 6 when using the S0S1S2 cube, which shows how both the detection and false alarms change based on the number of spectral bands.

In each case there are detections that occur in the background which will be defined in this analysis as any pixels that are not on vehicles. These will be called false alarms since the goal of this project is to find man-made anomalies. An interesting trade-off that is shown in this analysis is that of number of spectral bands vs. noise. As the number of spectral bands increases, greater separability can be achieved in the hyperspace allowing for better background / anomaly discrimination. However, as bands are averaged spectrally to create larger bandpasses, there is an increase in the system signal to noise ratio. The anomaly detection algorithm tends to produce lower false alarm levels in imagery that has lower noise. An example of this trade-off is shown in the difference between Figure 6(c) and 6(d). While the RGB image looses one spectral band, it has a better signal to noise ratio than the four band image and thus achieves fewer false alarms as seen in the detection maps.

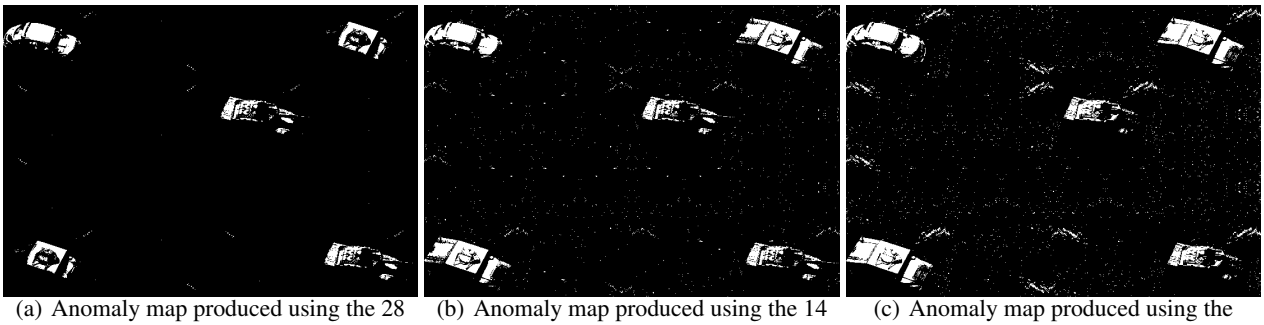

(a) Anomaly map produced using the 28 band S0S1S2 cube.

(b) Anomaly map produced using the 14 band S0S1S2 cube.

(c) Anomaly map produced using the WV2 4 band S0S1S2 cube.

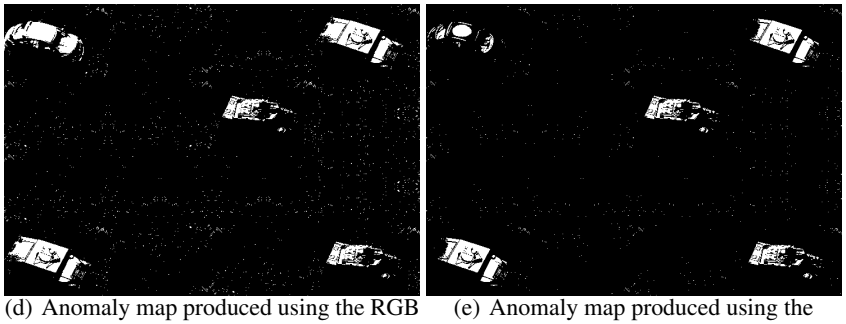

(d) Anomaly map produced using the RGB 3 band S0S1S2 cube.

(e) Anomaly map produced using the WV2 pan band image.

Figure 6: Anomaly detection maps produced by thresholding the TAD-RX score.

This approach was also applied to the S0 image cubes to show a comparison in algorithm performance between the spectro-polarimetric S0S1S2 data and intensity only cubes. The S0S1S2 data produces lower false alarm rates compared to S0 only data for each band combination which is shown in Figure 7. This is most apparent for the panchromatic case where even with a lack of spectral information, the algorithm can utilize the discriminability in the S1 and S2 bands to achieve a low false alarm rate. When using only S0, there is very little contrast in brightness values between the man-made objects and the background thus producing a very high false alarm rate.

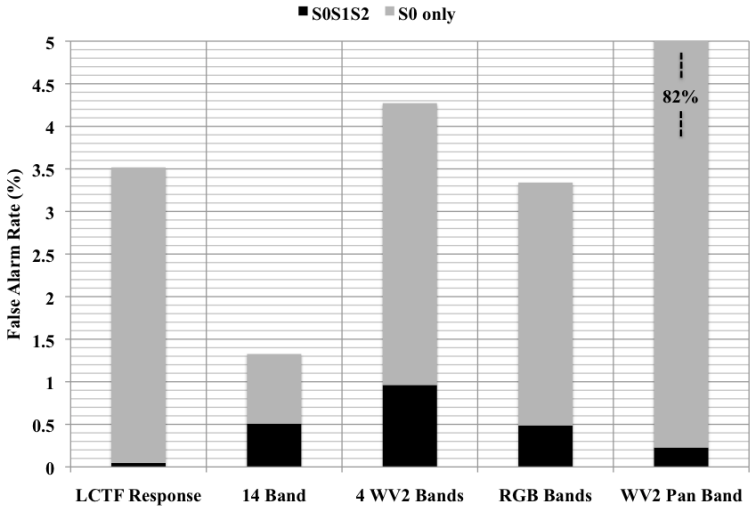


Figure 7: False alarm rate showing the number of false alarms as a percentage of the total image. Utilizing the S0S1S2 image cube allows for much lower rates in each spectral resolution case.

## 4. CONCLUSIONS

A new approach for combining spectro-polarimetric data for anomaly detection was presented that allows for direct application of spectral processing algorithms. In this case, a TAD-RX anomaly detection algorithm was applied to intensity only spectral image cubes as well as the combined S0S1S2 spectro-polarimetric image cube. The spectral response of data collected in the lab of a scale model scene was resampled to several different system responses. In each case, applying the algorithm to the combined S0S1S2 image cubes yielded a lower false alarm rate compared to intensity only data when classifying the man-made objects in the scene as anomalous.

While good anomaly detection results are realizable using a the single panchromatic S0S1S2 band, it should be noted that the source / target / detector geometries were aligned such that the polarimetric signal was maximized. The results should therefore be considered a best case scenario and further work should be done exploring the impact of moving the detector location out of the source / target principle plane as well as it's zenith viewing angle. As the polarimetric contrast is diminished due to varying geometries, the benefit of increased spectral resolution should become more apparent.

## REFERENCES


[1] Messinger, D., Ziemann, A., Basener, B., and Schlamm, A., "Spectral image complexity estimated through local convex hull volume," *accepted for publication in the Proceedings of the 2010 IEEE WHISPER Workshop* , IEEE (2010).

[2] Alouini, M., Goudail, F., Refregier, P., Grisard, A., Lallier, E., and Dolfi, D., "Multispectral polarimetric imaging with coherent illumination: towards higher image contrast," *Polarization: Measurement, Analysis, and Remote Sensing VI* **5432**(1), 133–144, SPIE (2004). [doi:10.1117/12.543620].

[3] Alouini, M., Goudail, F., Grisard, A., Bourderionnet, J., Dolfi, D., Bénière, A., Baarstad, I., Løke, T., Kaspersen, P., Normandin, X., and Berginc, G., "Near-infrared active polarimetric and multispectral laboratory demonstrator for target detection," *Appl. Opt.* **48**, 1610–1618 (Mar 2009). [doi:10.1364/AO.48.001610].

[4] Schott, J. R., [*Fundamentals of Polarimetric Remote Sensing* ], vol. TT81, SPIE Tutorial Texts In Optical Engineering (2009). [doi:10.1117/3.817304].

[5] Flusche, B. M., Gartley, M. G., and Schott, J. R., "Assessing the impact of spectral and polarimetric data fusion via simulation to support multimodal sensor system design requirements," *Journal of Applied Remote Sensing* **4**, 043562 (2010). [doi:10.1117/1.3525590].

[6] Bartlett, B. D., Gartley, M. G., Messinger, D. W., Salvaggio, C., and Schott, J. R., "Spectro-polarimetric bidirectional reflectance distribution function determination of in-scene materials and its use in target detection applications," *Journal of Applied Remote Sensing* **4**, 043552 (2010). [doi:10.1117/1.3518394].

[7] Bartlett, B. D. and Schlamm, A., "Anomaly detection with varied ground sample distance utilizing spectropolarimeter," *Optical Engineering* **50**(8) (2011).

[8] Reed, I. and Yu, X., "Adaptive multiple-band cfar detection of an optical pattern with unknown spectral distribution," *Acoustics, Speech and Signal Processing, IEEE Transactions on* **38**, 1760 –1770 (oct. 1990). [doi:10.1109/29.60107].

[9] Schott, J. R., [*Remote Sensing: The Imaging Chain Approach* ], ch. 10.2: Issues of Dimensionality and Noise, Oxford University Press, 2nd ed. (2007).

[10] Basener, B., Messinger, D., and Ientilucci, E., "Anomaly detection using topology," *Proc. SPIE* **6565** (2007). [doi:10.1117/12.745429].

[11] Basener, W. F. and Messinger, D. W., "Enhanced detection and visualization of anomalies in spectral imagery," *Algorithms and Technologies for Multispectral, Hyperspectral, and Ultraspectral Imagery XV* **7334**(1), 73341Q, SPIE (2009). [doi:10.1117/12.818672].

[12] Basener, W. F., "Clutter and anomaly removal for enhanced target detection," *Algorithms and Technologies for Multispectral, Hyperspectral, and Ultraspectral Imagery XVI* **7695**(1), 769525, SPIE (2010). [doi:10.1117/12.850303].